Biochemistry

Article

pubs.acs.org/biochemistry

Divalent Metal Ion Activation of a Guanine General Base in the Hammerhead Ribozyme: Insights from Molecular Simulations

Haoyuan Chen,[†] Timothy J. Giese,[†] Barbara L. Golden,[‡] and Darrin M. York*[,†]

[†]Laboratory for Biomolecular Simulation Research, Center for Integrative Proteomics Research, and Department of Chemistry & Chemical Biology, Rutgers University, 174 Frelinghuysen Road, Piscataway, New Jersey 08854-8076, United States

[‡]Department of Biochemistry, Purdue University, West Lafayette, Indiana 47907, United States

Supporting Information

ABSTRACT: The hammerhead ribozyme is a well-studied nucleolytic ribozyme that catalyzes the self-cleavage of the RNA phosphodiester backbone. Despite experimental and theoretical efforts, key questions remain about details of the mechanism with regard to the activation of the nucleophile by the putative general base guanine (G12). Straightforward interpretation of the measured activity−pH data implies the pK_a value of the N1 position in the G12 nucleobase is significantly shifted by the ribozyme environment. Recent crystallographic and biochemical work has identified pH-dependent divalent metal ion binding at the N7/O6 position of G12, leading to the hypothesis that this binding mode could induce a pK_a shift of G12 toward neutrality. We present computational results that support this hypothesis and provide a model that unifies the interpretation of available structural and biochemical data and paints a detailed mechanistic picture of the general base step of the reaction. Experimentally testable predictions are made for mutational and rescue effects on G12, which will give further insights into the catalytic mechanism. These results contribute to our growing knowledge of the potential roles of divalent metal ions in RNA catalysis.

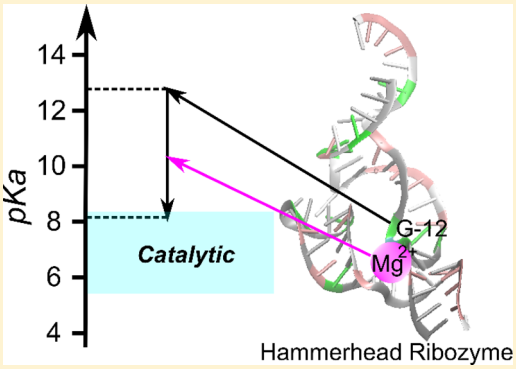

The hammerhead ribozyme (HHR) is a prototype catalytic RNA system that has been extensively studied[1−9] for almost three decades since it was first discovered by Uhlenbeck in 1987.[10] The HHR catalyzes the cleavage transesterification of the RNA sugar−phosphate backbone.[8] In the generally accepted acid−base mechanism, the nucleophile (the 2′-hydroxyl of residue C17) will donate a proton to a general base to form an activated precursor and attack the adjacent scissile phosphate, in a stepwise or partially concerted fashion. Departure of the O5′ leaving group is then facilitated by a general acid, leading to a 2′,3′-cyclic phosphate.[8]

Despite the wealth of structural,[11−16] biochemical,[6,17−40] and computational[3,8,41−49] data available, certain details about the catalytic mechanism remain unclear. In particular, the specific mechanism whereby the nucleophile becomes activated by a general base is not yet resolved. Biochemical studies[30,31,36] have suggested that the guanine nucleobase in residue G12 may act as the general base in HHR, which is also supported by crystal structures[13,15] in which the N1 site of G12 is well-positioned to interact with the 2′-hydroxyl group of C17 (Figure 1). Interestingly, guanine is observed to interact with the 2′-hydroxyl nucleophile in many other ribozyme systems,[9] including the hairpin,[50,51] glmS,[52,53] Varkud satellite,[54] twister,[55,56] and pistol[57] ribozymes, which thus appears to be a common theme in RNA catalysis.

A conceptual objection to the hypothesis that G12 may act as the general base is that the apparent pK_a values derived from activity−pH profiles (around 8[15,30,31,36]) are somewhat lower than the pK_a value of guanine in aqueous solution (9.2). To reconcile these observations, the most straightforward interpretation is that the pK_a of G12 would need to be considerably downshifted by the ribozyme active site. This prospect seems unlikely given the high degree of localized negative charge in the active site,[46] the proximity of G12 to the scissile phosphate, and the lack of nearby divalent metal ions in the active site of an earlier crystallographic structure with resolved solvent.[43]

Recently, a new set of crystal structures[15] of a full length hammerhead ribozyme (RzB) have been obtained that indicate a divalent ion (Mn^{2+}) is bound directly to the Hoogsteen face of G12 (inner sphere to N7) at pH 8 [Protein Data Bank (PDB) entry 5DI2]. In work that followed,[16] crystal structures of a vanadate transition state analogue at pH 8.2 were observed to have Mn^{2+} (PDB entry 5EAQ) and Mg^{2+} (PDB entry 5EAO) bound in a similar position, but directly coordinating O6. This binding mode is also similar to the position of an electron density peak found in the previous crystal structures at lower pH and interpreted as a likely water molecule[43] or Na^+ ion.[14]

Divalent metal ions have been predicted to be capable of considerably shifting the pK_a values of certain residues in the

Received: November 24, 2016
Revised: April 18, 2017
Published: May 22, 2017

DOI: 10.1021/acs.biochem.6b01192
Biochemistry XXXX, XXX, XXX−XXX

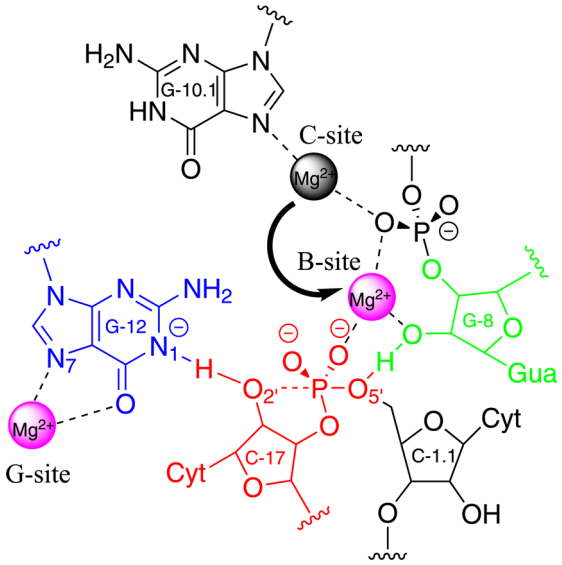

Figure 1. Illustration of the active site interactions in HHR and its self-cleavage mechanism. The N1 position of guanine in the putative general base G12 (blue) needs to be deprotonated before acting as a proton acceptor to deprotonate the 2′-OH in C17 (red), which will then act as the nucleophile to attack the phosphorus. Recent studies[15,16] indicate that there could be a Mg^{2+} directly bound (inner-sphere coordination) at the Hoogsteen face of G12 ("G-site") to facilitate its deprotonation. Another Mg^{2+} is believed to play the role of activating the 2′-OH of the general acid G8 (green) by migrating from the binding site at N7 of G10.1 ("C-site") observed crystallographically into a bridging position ("B-site") with the scissile phosphate, in accord with thio/rescue effect experiments.[29,39,58] In this bridging position, the Mg^{2+} can coordinate the 2′-OH of G8, increasing its acidity and facilitating the transfer of a proton to the O5′ leaving group in the general acid step of the reaction.[8] Alternative plausible roles for the G8:O2′ position along with a hydrated divalent metal ion acting as the general acid have been suggested,[16] and it is conceivable that there may be multiple competing pathways for acid catalysis that may vary with pH and ionic conditions.

ribozyme environment to facilitate catalysis.[59−61] Recently, Auffinger and co-workers conducted a database survey and suggested that Mg^{2+} ions do not bind to N7 on the Hoogsteen face of nucleobases with a few documented exceptions,[62,63] although other softer divalent ions such as Mn^{2+}, Zn^{2+}, and Cd^{2+} have been observed. Consequently, within the context of the ribozyme mechanism, it is of interest to gain a quantitative understanding of the degree to which different modes of binding of a divalent metal ion to guanine facilitate general base activation in nucleolytic ribozymes.

In this paper, we explore the feasibility of a divalent Mg^{2+} ion, bound to G12, to shift the pK_a at the N1 position as required by its implicated role as a general base in the reaction and make quantitative predictions that are experimentally testable. Electronic structure calculations are performed to quantify the magnitude of pK_a shifts induced by Mg^{2+} binding in several Mg^{2+}−guanine complexes and binding modes. Molecular dynamics (MD) simulations are performed with newly developed force field parameters for binding of a divalent metal ion to nucleic acids[64] to characterize the ribozyme active site environment, and thermodynamic integration (TI) is used to evaluate the pK_a shift of G12 in HHR with and without the Mg^{2+} bound. *Ab initio* quantum mechanical/molecular mechanical (QM/MM) simulations with rigorous long-range electrostatic interactions[65] are performed to explore the free energy profile for the general base step in the presence and absence of Mg^{2+} bound at the newly identified position. Taken together, these results are in quantitative agreement with available experimental data and support a mechanism whereby Mg^{2+} serves to stabilize G12 in an active (deprotonated) form that will ultimately facilitate deprotonation of the nucleophile in the general base step of the reaction. In addition, quantum mechanical calculations on the binding free energies between different divalent metal ions and guanine/6-thioguanine predict that a 6-thio substitution at G12 in HHR will decrease the catalytic reaction rate by eliminating Mg^{2+} binding while replacing Mg^{2+} with Mn^{2+} or Cd^{2+} could have rescue effects, which could be tested in future experimental works.

METHODS

Electronic Structure Calculations. All electronic structure calculations were performed in the Gaussian09 package[66] using the M06-2X[67] density functional with the 6-311++G(3df,3pd) basis set. The PCM solvation model[68−71] was used to treat the solvation effects, whose solvation cavity is constructed from the UFF radii set scaled by a factor of 1.1.[72] Harmonic vibrational analysis was performed on the optimized geometries using rigid rotor and harmonic oscillator approximations to verify the nature of the stationary points and obtain the thermal corrections to free energies. The relative pK_a values (i.e., the pK_a shifts) were calculated from

$$\Delta pK_a = (\Delta G' - \Delta G)/RT \ln(10) \quad (1)$$

where $\Delta G'$ and ΔG are the deprotonation reaction free energies of the Mg^{2+}−guanine complex and guanine, respectively. Free energy differences between two deprotonation reactions in kilocalories per mole were converted to pK_a shifts in pK_a units by dividing by RT ln(10). The pK_a shift is further corrected by taking the Mg^{2+} ion concentration and Mg^{2+}−guanine binding affinity into account. By considering a kinetic model that consists of deprotonation of guanine, the Mg^{2+}−guanine binding equilibrium, and deprotonation of the Mg^{2+}−guanine complex, we obtained estimates for the corrected pK_a of the Mg^{2+}−guanine complex as (see the Supporting Information for details, as well as Tables S1 and S2 for additional results)

$$pK_a(\mathrm{Mg-Gua,\ corr.}) = -\log_{10}\left[\frac{10^{-pK_a(\mathrm{Gua})} + c_{Mg} \times e^{-\beta\Delta G_{bind}} \times 10^{-pK_a(\mathrm{Mg:Gua,uncorr})}}{1 + c_{Mg} \times e^{-\beta\Delta G_{bind}}}\right] \quad (2)$$

where c_{Mg} is the concentration of Mg^{2+} ion (0.01 M was used in this work to be consistent with conditions in the crystal) divided by the standard molar concentration, 1.0 M (thus dimensionless), and ΔG_{bind} is the Mg^{2+}−guanine binding affinity that has been experimentally measured to be −0.34 kcal/mol[64,73] (see the Supporting Information for details). Electron population analysis was performed on the guanine and Mg^{2+}−guanine complex molecules (both neutral and deprotonated) at their optimized geometries using the natural bond orbital (NBO) analysis[74] method, as implemented in Gaussian09.

For the binding free energy calculations between different metal ions and guanine/6-thioguanine, the chemical equations that define the binding free energy are

$$M(H_2O)_6^{2+} + G \rightarrow [M(H_2O)_5{:}G]^{2+} + H_2O \quad (3)$$

DOI: 10.1021/acs.biochem.6b01192
Biochemistry XXXX, XXX, XXX−XXX

or

$$M(H_2O)_6^{2+} + G^- \rightarrow [M(H_2O)_5{:}G]^+ + H_2O \quad (4)$$

in which M could be Mg^{2+}, Mn^{2+}, or Cd^{2+} and G could be guanine or 6-thioguanine. For Mn and Cd atoms, the SDD effective core potential[75] was used. The cavity radii of the S atom were adjusted from 2.0175 (default as implemented in Gaussian09) to 2.6, which correctly reproduces the experimentally measured[76] pK_a between guanine and 6-thioguanine.

Molecular Dynamics Simulations. All molecular dynamics simulations were performed in the Amber14 package.[77] With the recent crystal structure of the RzB hammerhead ribozyme with a divalent metal ion bound at G12[15] at the starting point (PDB entry 5DI2), the RNA was solvated in a box of TIP4P-Ew[78] water molecules with a 12 Å buffer; 67 Na^+ and 15 Cl^- ions were added to neutralize the system and solvate it with 0.14 M NaCl (roughly physiological salt conditions). The RNA was treated with the AMBER-ff14SB force field,[79,80] which includes the corrections for α/γ conformers[81] and glycosidic torsions[82] in nucleic acids. The monovalent ions were described using the TIP4P-Ew-compatible parameters developed by Joung and Cheatham.[83] To better characterize the interaction between Mg^{2+} and nucleic acids, we apply the recently developed m12-6-4 parameter set developed by Panteva, Giambaşu, and York[64] to accurately describe balanced interactions between Mg^{2+} and nucleic acids. This model was based on pioneering work by Li and Merz[84] to include effects of ion-induced polarization, using a simple pairwise approximation that does not require further alteration of conventional molecular simulation force fields. This model provides outstanding agreement with structural, thermodynamic, kinetic, and mass transport properties of Mg^{2+} in aqueous solution[85] and has recently been extended to give balanced interactions with nucleic acids through adjustment of specific pairwise parameters.[64] This model was used to describe all six Mg^{2+} ions that were present in the crystal structure and in the simulations. The system was then slowly heated to 300 K and equilibrated for a total simulation time of >30 ns (termed HHR·Mg^{2+}:G12). To justify the effect of the G12-bound Mg^{2+}, another system was built by removing the G12-bound Mg^{2+} and went through the same equilibration process (termed HHR:G12). Also, a reference system was set up by solvating a single guanosine monophosphate residue (CH_3-capped at the O3′ position and CH_3O-capped at the P position) in a box of TIP4P-Ew water with a 20 Å buffer along with 13 Na^+ and 12 Cl^- ions. This system was heated to 300 K and equilibrated for a total simulation time of 5 ns. All simulations employ an 8 Å nonbond cutoff and make use of particle mesh Ewald to account for the electrostatics beyond the cutoff.[86]

Thermodynamic Integration Calculations. With the equilibrated structures as the starting point, all three systems (solvated guanosine, HHR:G12, and HHR·Mg^{2+}:G12) were prepared for thermodynamic integration (TI) calculations to compute the free energy of deprotonating guanine or G12. The net free energy change is $\Delta G_{DEPR} = G_{G^-} - G_{GH}$, where G_{GH} is the free energy of the neutral guanine state (both in the reference system and at the G12 position in the HHR) and G_{G^-} is the free energy of the guanine deprotonated at the N1 position, which carries a net charge of −1. To stably compute the net free energy change from a reasonable amount of statistical sampling, it is advantageous to decompose the free energy change as a sum of three stages[87] that pass through intermediate states:

$$\Delta G_{DEPR} = \Delta G_{decharge} + \Delta G_{bond\text{-}removal} + \Delta G_{recharge} \quad (5)$$

where $\Delta G_{decharge}$, $\Delta G_{bond\text{-}removal}$, and $\Delta G_{recharge}$ are termed the "decharging", "bond-removal", and "recharging" stages, respectively. The advantage of this decomposition is that less sampling than what would otherwise be necessary is required to compute each stage through a direct transformation between the two end states. In the decharging stage, the partial charge on H1 is removed. In the bond-removal stage, the bond, angle, torsion, and Lennard-Jones interaction terms in the force field involving H1 are removed. In the recharging stage, the partial charges on the entire residue are transformed to the charge set for the deprotonated guanine derived from RESP charge fitting.[88] The free energy of each stage is computed from TI:

$$\Delta G_{stage} = \int_0^1 \left\langle \frac{\partial \mathcal{H}_{stage}(\lambda)}{\partial \lambda} \right\rangle_\lambda d\lambda \quad (6)$$

where $\mathcal{H}_{stage}(\lambda)$ is a linear combination of Hamiltonians that define the end states of the stage:

$$\mathcal{H}_{stage}(\lambda) = (1-\lambda)\mathcal{H}^{(0)}_{stage} + \lambda \mathcal{H}^{(1)}_{stage} \quad (7)$$

where $\mathcal{H}^{(0)}_{stage}$ and $\mathcal{H}^{(1)}_{stage}$ are the Hamiltonians for the stage's initial and final states, respectively. As an exception to eq 7, the removal of the Lennard-Jones interaction within the "bond-removal" stage is performed through a nonlinear "soft-core" potential:[64,89]

$$V_{sc}(\lambda) = 4\varepsilon(1-\lambda)\left\{\frac{1}{[\alpha\lambda + (r/\sigma)^6]^2} - \frac{1}{\alpha\lambda + (r/\sigma)^6}\right\} \quad (8)$$

where ε and σ are standard Lennard-Jones parameters, r is atomic distance, and α is an adjustable constant that was set to 0.5 by default.[89] The free energy change of each stage is evaluated by performing 11 simulations (TI "windows") corresponding to 11 evenly spaced values of λ, and numerically integrating eq 6 from the trapezoid rule. Each TI window is equilibrated for 100 ps at λ = 0.5, and statistics are sampled from 1 ns of production simulation.

The TI calculations described above involve 33 TI window simulations per system (3 stages/system and 11 windows/stage) to compute a net free energy change. To ascertain the reliability of the result, we perform the procedure three times for each system (99 windows/system) to compute three estimates of the system's net free energy change. For each system, we report (see Table 3) the average ΔG_{DEPR} value and its standard error from the three estimates.

Quantum Mechanical/Molecular Mechanical Simulations. After G12 is deprotonated, it is suited to act as a general base that activates the nucleophile by facilitating the transfer of a proton from the nucleophile C17:O2′ to G12:N1. *Ab initio* QM/MM umbrella sampling simulations were performed to obtain the free energy profile of the proton transfer reaction for both HHR:G12 and HHR·Mg^{2+}:G12. The PBE0 hybrid density functional[90,91] with the 6-31+G(d) basis set was used to model the 47-atom (HHR:G12) or 48-atom (HHR·Mg^{2+}:G12) QM region. The QM region includes the guanine base in the G12 residue, the Mg^{2+} bound at G12 (but not the coordinating water molecules), and the entire C17 residue (cytosine base, sugar, and phosphate). The simulations were performed with an 8 Å nonbond cutoff, and the ambient-potential composite

DOI: 10.1021/acs.biochem.6b01192
Biochemistry XXXX, XXX, XXX−XXX

Ewald method[65] was used to describe the long-range electrostatics in the system.

The reaction coordinate ($\xi = R_1 - R_2$) is the difference between two distances. R_1 is the distance from proton donor C17:O2′ to proton C17:HO2′, and R_2 is the distance from proton acceptor G12:N1 to proton C17:HO2′. The umbrella biasing potential is

$$U_{bias}(\xi) = k(\xi - \xi_0)^2 \quad (9)$$

where ξ_0 is the reference coordinate for the window and k (=50 kcal mol^{-1} Å^{-2}) is a force constant. Each profile is generated from 16 simulation windows whose reference coordinate (ξ_0) evenly samples the range from −1.6 to 1.4 Å. Each window is equilibrated for 2.5 ps, and statistics were drawn from 10 ps of production simulation. The statistics gathered from the biased simulations are analyzed using the variational free energy profile (vFEP) method[92] to generate the unbiased free energy profiles.

RESULTS AND DISCUSSION

Guanine nucleobases are often encountered in ribozyme active sites and have been implicated as acting as the general base in catalysis. To act as a general base, the guanine nucleobase should be activated by deprotonation at the N1 position (Figure 2). In the deprotonated state, resonance stabilization

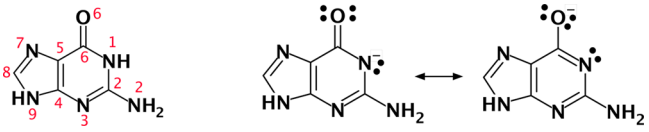

Figure 2. Canonical numbering (left) of the guanine nucleobase and resonance structures (right) of guanine deprotonated at the N1 position with formal charge alternately on N1 and O6.

allows the negative charge to be distributed between the N1 and O6 positions. Divalent metal ion binding at the O6 position, therefore, would be expected to have a strong influence on the microscopic pK_a at the N1 position by stabilizing the deprotonated form. In the following sections, we build up models for binding of Mg^{2+} to guanine and related chemically modified analogues used in mechanistic experiments and make predictions about the induced pK_a shift at the N1 position and on the free energy of the general base step in the chemical reaction.

pK_a Shifts of Mg^{2+}−Guanine Complexes. To obtain a more detailed picture of the Mg^{2+}−guanine interaction and its effect on the pK_a, we designed model compounds that mimic the divalent metal ion−guanine complex in the HHR crystal structure (PDB entry 5DI2)[15,16] (in some cases, the divalent ion was Mn^{2+}) and performed density functional electronic structure calculations. To validate the computational protocol and quantum chemical model chemistry, we calculated the pK_a shifts of three chemically modified guanines: substitution of N3/N7 with CH, which makes 3/7-deazaguanine, and replacement of exocyclic NH_2 with H, which yields inosine (Figure 3). From Table 1, the calculated pK_a shifts of all three chemically modified guanines agree very well with experimental values (maximal error of 0.4 pK_a unit).

Next, we examined several Mg^{2+}−guanine model complexes that mimicked the metal ion binding mode observed in the crystal structure of reactant state HHR (PDB entry 5DI2) in which the hexacoordinated Mg^{2+} has inner-sphere contact with N7 and outer-sphere coordination with O6 (Figure 4). We also

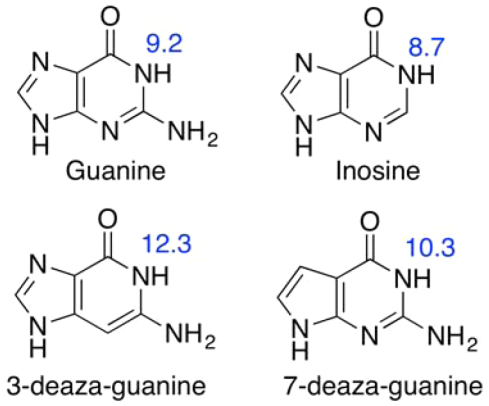

Figure 3. Chemical structures of guanine and several chemically modified guanine molecules studied in this work. Experimental pK_a values at the N1 position (taken from refs 93 and 94) are shown.

Table 1. Calculated and Experimental pK_a Shifts of Guanine, Chemically Modified Guanine, and Mg^{2+}−Guanine Complexes[a]

model	pK_a shift (calcd)	pK_a shift (exptl)
guanine (reference)	–	–
inosine	−0.3	−0.5[93]
3-deazaguanine	3.2	3.1[94]
7-deazaguanine	1.5	1.1[94]
Mg^{2+}−$(H_2O)_5$−guanine	−7.0	–
Mg^{2+}−$(H_2O)_5$−inosine	−7.0	–
Mg^{2+}−$(H_2O)_5$−3-deazaguanine	−4.4	–
HHR G12	–	−1.2[15]

[a]The calculated pK_a shifts have been corrected for Mg^{2+}−guanine binding affinity and Mg^{2+} concentration (0.01 M) using eq 2. Error estimates are not available because the methods used to obtain those values are deterministic and do not involve sampling.

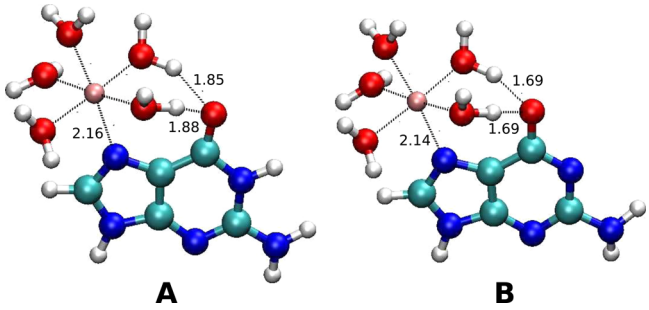

Figure 4. Optimized geometries of (A) Mg^{2+}−guanine and (B) Mg^{2+}−deprotonated guanine complexes. Selected bond lengths shown are in angstroms.

picked two of the three chemically modified species (3-deazaguanine and inosine) and built complexes with Mg^{2+} in the same way. These two species were chosen because, unlike the 7-deaza modification, neither directly alters the chemical environment of the Hoogsteen face, therefore preserving the observed binding mode of the native guanine. For 7-deazaguanine, it is expected that Mg^{2+} binding would be considerably disrupted. As seen in Table 1, the magnitude of pK_a shifts induced by Mg^{2+} (≈−7 pK_a units) is quite large, making the N1 position considerably more acidic. This large shift agrees with previous arguments[59,61,95] that metal ion binding could induce large pK_a shifts of nucleobase residues.

DOI: 10.1021/acs.biochem.6b01192
Biochemistry XXXX, XXX, XXX−XXX

Table 2. Partial Atomic Charges of Selected Atoms in Guanine and Mg^{2+}−Guanine Complexes Derived from NBO Analysis

model	N1	H1	N3	O6	N7	guanine
guanine	−0.663	0.472	−0.603	−0.687	−0.510	0.000
Mg^{2+}−$(H_2O)_5$−guanine	−0.635	0.484	−0.582	−0.743	−0.582	0.168
(difference)	(0.028)	(0.012)	(0.021)	(−0.056)	(−0.071)	(0.168)
guanine(−)	−0.716	–	−0.659	−0.792	−0.533	−1.000
Mg^{2+}−$(H_2O)_5$−guanine(−)	−0.651	–	−0.617	−0.830	−0.602	−0.767
(difference)	(0.065)	–	(0.042)	(−0.038)	(−0.069)	(0.233)

The experimentally observed pK_a shift of G12 in the ribozyme environment is a much smaller shift toward neutrality (≈−1.2 pK_a units[15]). As will be discussed in more detail in the next section, the accumulated negative charge of the ribozyme active site in the hammerhead ribozyme leads to a considerable positive pK_a shift that requires binding of a divalent metal ion at the G-site to offset the shift. The main point of this section is to establish a baseline for the expected pK_a shifts that a Mg^{2+} would be expected to induce if it were bound to an isolated guanine (or modified guanine) nucleobase in solution, before making predictions about the pK_a shifts in the more complex active site of the HHR.

To examine the effect of Mg^{2+} binding on the electronic structure of guanine, we performed NBO analysis to calculate the partial atomic charges in the neutral and deprotonated species (Table 2). Of the key atoms listed, the largest negative charge is seen to reside at the O6 position in both protonation states and in the presence and absence of Mg^{2+}. Position O6 exhibits the greatest increase in negative charge upon deprotonation, in the presence and absence of Mg^{2+}. The charge at the O6 position is also seen to grow considerably more negative for both neutral and deprotonated guanine, upon Mg^{2+} binding, but not as dramatically as at the N7 position where the ion has direct inner-sphere coordination. Overall, the transfer of charge from guanine to the hydrated Mg^{2+} ion is relatively modest for both neutral and deprotonated (anionic) guanine (0.17 and 0.23 *e*, respectively). These results indicate that the interaction between Mg^{2+} and guanine is mostly electrostatic in nature, providing justification for the use of fixed-charge molecular mechanical (MM) force fields to model the Mg^{2+}−guanine interaction that will be introduced in the next subsection.

pK_a Shift of G12 in HHR. To better characterize the effects of the complicated enzyme environment, MD simulation of the full HHR was conducted and the pK_a shift of guanine N1 position in G12 was then evaluated using TI (Figure 5). The

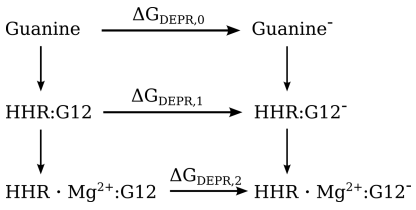

Figure 5. Thermodynamic cycle used in TI calculations.

reference system was the deprotonation of a single guanine nucleotide in solution that has a known experimental pK_a of 9.2. For the HHR system, both HHR:G12 and HHR·Mg^{2+}:G12 were simulated. The two pK_a shift values were then determined using eq 1. This approach has been adopted to predict pK_a shifts in ribozymes induced by the enzyme environments[56,96] and a closely related protein enzyme system in which the leading factor in the pK_a shift was also a Mg^{2+}[101] in previous works and was shown to give reasonable results.

As seen in Table 3, the simulations predicted that in HHR·Mg^{2+}:G12, the pK_a of N1 in G12 is shifted down by −1.2, while in HHR:G12, the pK_a is shifted up by 3.7 units. The convergence of the TI simulations in terms of the target observable pK_a shifts was measured (Figure 6) and showed that

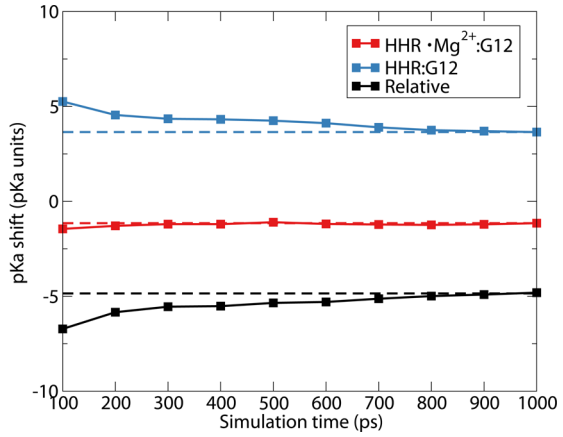

Figure 6. Convergence of pK_a shift values from TI simulations. Filled squares connected by solid lines are the pK_a shift values evaluated using all available data at a certain simulation time, with an increment of 100 ps per point. Dashed lines are drawn to help show the convergence.

the simulations reached reasonable convergence after 1 ns, which was similar to the time scales investigated in related work.[56,96,101] Experimental activity−pH profiles indicate that the apparent pK_a of the general base in HHR is around 8 in the presence of Mg^{2+}.[15] If guanine is assumed to be the general base, and the most straightforward interpretation of the apparent pK_a values is made, this would imply an expected shift in the pK_a of G12 by approximately −1.2 units (Figure 7).

As mentioned above, an electron density peak was found in the vicinity of G12 in the previous crystal structure of HHR obtained at pH 6.5[43] (PDB entry 2OEU) and was interpreted as a solvent water molecule. In a recent work,[15] the G12-bound Mg^{2+} was found in the crystal obtained at pH 8.0 but not in the one obtained at pH 5.0. Here, we analyzed the solvent distribution around the O6 position of G12 from the HHR:G12 simulations by calculating the radial distribution functions (RDFs). As seen in Figure 8, there is a clear peak around 2.6 Å in both RDFs, which is consistent with the previous structure in which the oxygen in the G12-bound water is 2.54 Å from O6 of G12. Also, in the RDF where G12 is deprotonated, the height of the peak is greater than when G12 is neutral, which suggests that the deprotonated G12, which is carrying a −1 charge, needs stronger electrostatic interactions to stabilize the negative charges that are buiding up on O6 and

DOI: 10.1021/acs.biochem.6b01192
Biochemistry XXXX, XXX, XXX−XXX

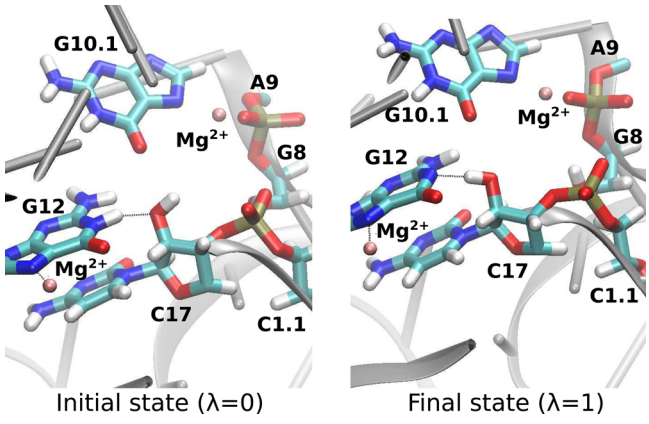

Figure 7. Representative active site conformation of the initial (left) and final (right) states from the free energy (TI) simulation of HHR·Mg^{2+}:G12. The conformations from the simulation of HHR:G12 are very similar and therefore not shown. For the sake of clarity, water molecules and some other atoms and/or residues are not displayed. White, cyan, blue, red, pink, and gold spheres stand for H, C, N, O, Mg, and P atoms, respectively.

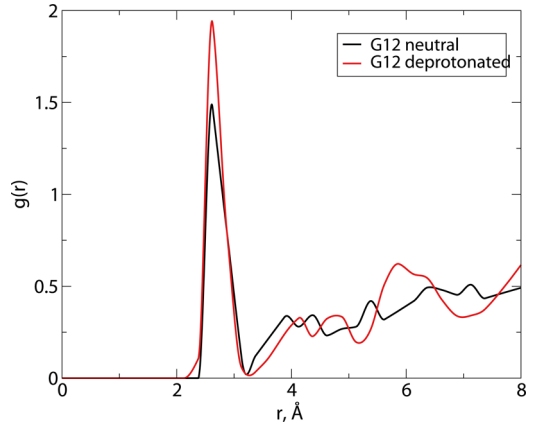

Figure 8. Radial distribution function (RDF) of water oxygens around the O6 position of neutral and deprotonated G12 in HHR. Both sets of data are extracted from 1 ns of MD simulation of HHR:G12 with G12 in neutral and deprotonated forms, respectively. RDF data points are calculated using window size of 0.2 Å and are interpolated using the Akima spline.

N7 than the neutral form does. These results indicate that the Mg^{2+}–G12 binding in HHR might have a pH dependence, which could be the reason why the G12-bound Mg^{2+} is found in only high-pH crystal structures but not in a low-pH crystal structure.

Taken together, the results reported here are consistent with a model in which a Mg^{2+} ion binds at the G-site and results in an overall pK_a shift of G12 toward neutrality by 1.2 pK_a units. In the absence of the metal ion binding at the G-site, the pK_a of G12 is predicted to be considerably shifted to higher pK_a values (12.9), making it unlikely to be activated as the general base in the biologically relevant pH range. This scenario would contradict the interpretation of activity–pH data in terms of apparent pK_a values. The fact that our calculated result is in striking agreement with experiment suggests that the apparent pK_a values observed experimentally may have this straightforward interpretation.

These results are consistent with previous calculations that indicate that HHR folds to form an electrostatically strained active site, which acts as an electronegative recruiting pocket for a threshold cationic charge required for efficient activity.[46] If the local environment around G12 in HHR is overall negatively charged, then it is expected that the pK_a of G12 will be shifted up in HHR compared to in aqueous solution. Via the recruitment of divalent metal ions, this shift is offset and even reversed. By comparing the pK_a shifts with and without Mg^{2+} in Table 3, we can estimate the net effect of Mg^{2+} on the pK_a of G12 to be −1.2 − 3.7 = −4.9 pK_a units, which is in qualitative agreement with our DFT result (−7.0). In the hepatitis delta virus (HDV) ribozyme, which has a similar divalent metal ion requirement under physiological conditions, a pK_a shift that is similar in magnitude (∼−4 units) on the 2′-hydroxyl nucleophile induced by Mg^{2+} was predicted by 3D-RISM calculations.[102] In addition, Amaro and co-workers have reported the Mg^{2+}-induced pK_a shift of lysine K82 in guanylyltransferase mRNA capping enzyme to be −4.2,[101] which is very close to the result reported here using a similar TI approach. Rosta and co-workers have also observed that Mg^{2+} plays the role of altering the pK_a in dUTPase, which catalyzes phosphate hydrolysis.[103,104]

Table 3. Deprotonation Free Energies (kilocalories per mole), pK_as, and pK_a Shifts (in pK_a units) of G12 in HHR from Different Sets of TI Simulations and Experiments

model	ΔG_{DEPR}	pK_a	pK_a shift
guanine (reference)	−114.1 ± 0.5	9.2	–
HHR:G12	−108.9 ± 0.3	12.9 ± 0.2	3.7 ± 0.2
HHR·Mg^{2+}:G12	−115.8 ± 0.5	8.0 ± 0.4	−1.2 ± 0.4
experiments[15]	–	8.0	−1.2

It is noteworthy that, at high concentrations (≥ 1.0 M) of monovalent salts, HHR can undergo self-cleavage in the absence of divalent metal ions with only a modest decrease in rate.[97−99] It is conceivable that at high monovalent salt concentrations, cationic charge stabilization at the G12:O6 position might produce a catalytic effect similar to that of divalent metal ion binding. Alternatively, it may be the case that under high-salt conditions, a different mechanism is available, although it is likely that at least a small part of the full HHR rate enhancement does require at least one divalent metal ion.[99] Very recently, more probing study of the dependence of HHR kinetics on ionic conditions has shed light on these and other important mechanistic details and suggests a cooperative interaction involving the nucleophilic 2′-OH, G12, the −1 nucleobase C17, and Mg^{2+} ions.[100]

Free Energy Profile for the General Base Step. From TI-MD simulations, we found that the G12-bound Mg^{2+} in HHR could activate the general base G12 by downshifting its pK_a to facilitate its deprotonation. Nonetheless, because the next step after general base activation is the transfer of a proton from the nucleophile to the general base, one might expect that having a Mg^{2+} bound at G12 could make this step thermodynamically less favorable because binding of Mg^{2+} to deprotonated G12 makes it a worse proton acceptor. One possibility is that the Mg^{2+} could "leave the scene" after the deprotonation of G12 to avoid the energy penalty in the following step. However, in the crystal structure of the vanadate transition state mimic[16] (PDB entries 5EAQ and 5EAO) that mimics the state after the general base proton transfer step is completed, the divalent ion was still found to be bound at G12. This suggested that the Mg^{2+} might be bound at G12 all the

DOI: 10.1021/acs.biochem.6b01192
Biochemistry XXXX, XXX, XXX−XXX

time despite the energy penalty of the general base proton transfer step, which could potentially be compensated by providing electrostatic stabilization to the overall negatively charged active site.

To evaluate the energy penalty induced by Mg^{2+}, we performed *ab initio* QM/MM umbrella sampling simulations of the general base proton transfer step for both HHR:G12 and HHR·Mg^{2+}:G12. As shown in Figure 9, the reaction in HHR·

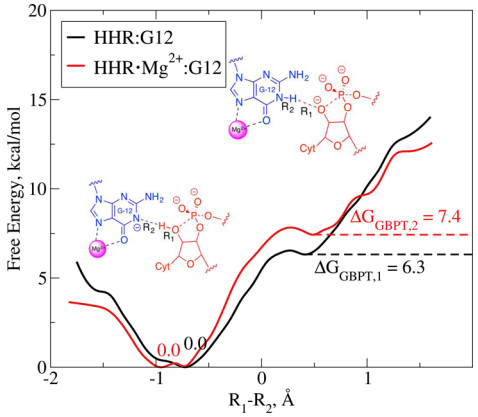

Figure 9. Free energy profile for the general base proton transfer (GBPT) reaction in HHR·Mg^{2+}:G12 (red) and HHR:G12 (black) generated by *ab initio* QM/MM umbrella sampling. The two chemical structures depict the reactant (left) and product (right) states. The reaction coordinate is the difference ($R_1 - R_2$) between the distance from C17 O2′ to C17 HO2′ (R_1) and the distance from G12 N1 to C17 HO2′ (R_2). Relative free energies of the reactant and product states are marked.

Mg^{2+}:G12 did have a higher free energy cost. However, the decrease in the free energy cost of the G12 deprotonation induced by Mg^{2+} was more than enough to compensate for this (Table 4). Overall, the free energy required for the system to

Table 4. Summary of Predicted Free Energy Costs in Different Steps for HHR:G12 and HHR·Mg^{2+}:G12[a]

model	ΔG_{DEPR}	ΔG_{GBPT}	ΔG_{TOTAL}
HHR:G12	6.7 ± 0.6	6.3 ± 0.2	13.0 ± 0.6
HHR·Mg^{2+}:G12	0.0 ± 0.0	7.4 ± 0.2	7.4 ± 0.2

[a]Relative ΔG_{DEPR} values are taken from Table 3, while ΔG_{GBPT} values are from QM/MM free energy profiles as labeled in Figure 9. All numbers are in kilocalories per mole. Error estimates for ΔG_{DEPR} values are from Table 3, while for ΔG_{GBPT}, they are from bootstrapping (see the Supporting Information for details). Standard errors of ΔG_{TOTAL} are obtained using the propagation rule.

reach the state that is ready for phosphoryl transfer is 5.6 kcal/mol lower when a G12-bound Mg^{2+} is present, which supports the existence and catalytic effect of a Mg^{2+} ion bound at the G-site in HHR.

Effect of 6-Thio Substitution on G12 and Rescue Effects. All the results and discussions mentioned above support the hypothesis that the G-site Mg^{2+} could facilitate the catalysis by downshifting the pK_a of G12. To further test the hypothesis and make predictions that could be directly tested by experiments, we examined the effects of changing a guanine to a 6-thioguanine. The 6-thioguanine molecule (sometimes termed tioguanine) has been used in medications for the treatment of leukemia and other diseases but has not, to the best of our knowledge, been used extensively as a mechanistic probe in ribozymes. The pK_a of 6-thioguanine has been experimentally measured to be 8.3,[76] almost a full unit lower than the pK_a of guanine (9.2). In a mechanistic scenario whereby there is no divalent metal ion bound at the G-site, one would expect the lower pK_a of 6-thioguanine would lead to slightly increased activity at neutral pH because of the higher probability of being in deprotonated form and able to accept a proton from the nucleophile in the general base step, and the activity−pH profile would be accordingly shifted. If, however, a divalent metal ion did bind at the G-site, thio substitution at position 6 could create a thio/rescue effect scenario.

To test this, we employed electronic structure calculations to obtain the binding free energies of Mg^{2+}, Mn^{2+}, and Cd^{2+} ions to guanine and 6-thioguanine, in neutral and deprotonated (at the N1 position) forms. Results are listed in Table 5, including

Table 5. Comparison of Estimated Binding Free Energies (kilocalories per mole) between Different Divalent Metal Ions and Guanine/6-Thioguanine in Neutral and Deprotonated Forms[a]

metal	guanine	guanine$^-$	6-thioguanine	6-thioguanine$^-$
Mg^{2+}	−0.3	−11.7	6.4	5.0
Mn^{2+}	−0.6	−12.4	0.7	−0.7
Cd^{2+}	−2.0	−10.8	−3.2	−4.5

[a]Values in the second column are converted from experimental binding affinities.[64,73] In each row, the values are normalized according to the corresponding experimental values in the second column.

normalization adjustments such that binding free energies are relative to guanine in its normal protonation state at neutral pH, and the column corresponding to guanine is taken from the experimental binding affinities.[64,73] Mg^{2+}−6-thioguanine binding is unfavorable relative to Mg^{2+}−guanine binding and suggests that the G-site Mg^{2+} could be knocked out upon 6-thio substitution at G12. Mn^{2+} and Cd^{2+}, which are softer, more thiophilic ions, show binding to 6-thioguanine more favorable than that of Mg^{2+}, which implies a partial rescue effect to the 6-thio substitution at G12 upon replacement of Mg^{2+} with Mn^{2+} and particularly Cd^{2+}. This is an experimentally testable prediction that could help to further reconcile the role of divalent metal ions in general base activation.

CONCLUSIONS

This work presents a series of quantum chemical calculations and molecular simulations to probe the activation mode of the general base in the hammerhead ribozyme (HHR). The hypothesis, motivated by recent crystallographic data, is that the presumed general base G12 is activated by a Mg^{2+} ion causing a pK_a shift toward neutrality that would allow it to have an increased probability of being in an ionized state where the N1 position can extract a proton from the 2′-OH nucleophile. The electronic structure calculations on small model systems suggest that a Hoogsteen face-bound Mg^{2+} ion could greatly downshift the pK_a of the N1 position in guanine, primarily because of electrostatic interactions. Free energy simulations in the full ribozyme environment strongly support a model in which the pK_a of G12 in HHR is shifted by a Mg^{2+} ion bound at the experimentally observed G-site by −1.2 units, in agreement with the apparent pK_a value derived from measured activity−pH profiles. QM/MM simulations of the general base proton transfer reaction further support the catalytic significance of this

DOI: 10.1021/acs.biochem.6b01192
Biochemistry XXXX, XXX, XXX−XXX

metal ion binding mode, and the role of the G-site Mg^{2+}. On the basis of binding free energy calculations, 6-thio substitution on G12 is predicted to reduce the catalytic activity but could be partially rescued by replacing Mg^{2+} with more thiophilic metal ions, which could be tested by experiments that measure the metal ion dependence on activity−pH profiles for chemically modified HHRs. The suggested role of metal ions in the activation of a guanine general base may represent a general catalytic strategy used by other RNA enzymes.

■ ASSOCIATED CONTENT

Supporting Information

The Supporting Information is available free of charge on the ACS Publications website at DOI: 10.1021/acs.biochem.6b01192.

Additional computational details (ZIP)

■ AUTHOR INFORMATION

Corresponding Author

*E-mail: darrin.york@rutgers.edu.

ORCID

Darrin M. York: 0000-0002-9193-7055

Funding

The authors are grateful for financial support provided by the National Institutes of Health (Grants GM062248 to D.M.Y. and GM095923 to B.L.G.).

Notes

The authors declare no competing financial interest.

■ ACKNOWLEDGMENTS

Computational resources were provided by the National Institutes of Health under Grant S10OD012346 and by the Extreme Science and Engineering Discovery Environment (XSEDE), which is supported by National Science Foundation Grant OCI-1053575 (Project TG-MCB110101 to D.M.Y.).

■ REFERENCES

(1) Scott, W. G. (1998) RNA catalysis. *Curr. Opin. Struct. Biol. 8*, 720−726.

(2) Kuimelis, R. G., and McLaughlin, L. W. (1998) Mechanisms of Ribozyme-Mediated RNA Cleavage. *Chem. Rev. 98*, 1027−1044.

(3) Zhou, D.-M., and Taira, K. (1998) The Hydrolysis of RNA: From Theoretical Calculations to the Hammerhead Ribozyme-Mediated Cleavage of RNA. *Chem. Rev. 98*, 991−1026.

(4) Scott, W. G. (1999) Biophysical and biochemical investigations of RNA catalysis in the hammerhead ribozyme. *Q. Rev. Biophys. 32*, 241−294.

(5) Takagi, Y., Ikeda, Y., and Taira, K. (2004) Ribozyme Mechanisms. *Top. Curr. Chem. 232*, 213−251.

(6) Blount, K. F., and Uhlenbeck, O. C. (2005) The Structure-Function Dilemma of the Hammerhead Ribozyme. *Annu. Rev. Biophys. Biomol. Struct. 34*, 415−440.

(7) Lilley, D. M., and Eckstein, F., Eds. (2008) *Ribozymes and RNA Catalysis*, RSC Biomolecular Series, RSC Publishing, Cambridge, U.K.

(8) Lee, T.-S., Wong, K.-Y., Giambasu, G. M., and York, D. M. (2013) *Prog. Mol. Biol. Transl. Sci. 120*, 25−91.

(9) Ward, W. L., Plakos, K., and DeRose, V. J. (2014) Nucleic acid catalysis: metals, nucleobases, and other cofactors. *Chem. Rev. 114*, 4318−4342.

(10) Uhlenbeck, O. (1987) A small catalytic oligoribonucleotide. *Nature 328*, 596−600.

(11) Pley, H. W., Flaherty, K. M., and McKay, D. B. (1994) Three-dimensional structure of a hammerhead ribozyme. *Nature 372*, 68−74.

(12) Scott, W. G., Finch, J. T., and Klug, A. (1995) The Crystal Structure of an All-RNA Hammerhead Ribozyme:A Proposed Mechanism for RNA Catalytic Cleavage. *Cell 81*, 991−1002.

(13) Martick, M., and Scott, W. G. (2006) Tertiary contacts distant from the active site prime a ribozyme for catalysis. *Cell 126*, 309−320.

(14) Anderson, M., Schultz, E. P., Martick, M., and Scott, W. G. (2013) Active-Site Monovalent Cations Revealed in a 1.55- Å-Resolution Hammerhead Ribozyme Structure. *J. Mol. Biol. 425*, 3790−3798.

(15) Mir, A., Chen, J., Robinson, K., Lendy, E., Goodman, J., Neau, D., and Golden, B. L. (2015) Two Divalent Metal Ions and Conformational Changes Play Roles in the Hammerhead Ribozyme Cleavage Reaction. *Biochemistry 54*, 6369−6381.

(16) Mir, A., and Golden, B. L. (2016) Two Active Site Divalent Ions in the Crystal Structure of the Hammerhead Ribozyme Bound to a Transition State Analogue. *Biochemistry 55*, 633−636.

(17) Dahm, S. C., and Uhlenbeck, O. C. (1991) Role of divalent metal ions in the hammmerhead RNA cleavage reaction. *Biochemistry 30*, 9464−9469.

(18) Tuschl, T., Ng, M. M., Pieken, W., Benseler, F., and Eckstein, F. (1993) Importance of exocyclic base functional groups of central core guanosines for hammerhead ribozyme activity. *Biochemistry 32*, 11658−11668.

(19) Tuschl, T., and Eckstein, F. (1993) Hammerhead ribozyme: Importance of stem-loop II for activity. *Proc. Natl. Acad. Sci. U. S. A. 90*, 6991−6994.

(20) Tuschl, T., Gohlke, C., Jovin, T. M., Westhof, E., and Eckstein, F. (1994) A three-dimensional model for the hammerhead ribozyme based on fluorescense measurements. *Science 266*, 785−789.

(21) Kuimelis, R. G., and McLaughlin, L. W. (1995) Hammerhead ribozyme-mediated cleavage of a substrate analogue containing an internucleotidic bridging 5′-phosphorothioate: implications for the cleavage mechanism and the catalytic role of the metal cofactor. *J. Am. Chem. Soc. 117*, 11019−11020.

(22) Kuimelis, R. G., and McLaughlin, L. W. (1996) Ribozyme-Mediated Cleavage of a Substrate Analogue Containing an Internucleotide-Bridging 5′-Phosphorothioate: Evidence for the Single-Metal Model. *Biochemistry 35*, 5308−5317.

(23) Baidya, N., and Uhlenbeck, O. C. (1997) A kinetic and thermodynamic analysis of cleavage site mutations in the hammerhead ribozyme. *Biochemistry 36*, 1108−1114.

(24) Scott, E. C., and Uhlenbeck, O. C. (1999) A re-investigation of the thio effect at the hammerhead cleavage site. *Nucleic Acids Res. 27*, 479−484.

(25) Morrissey, S. R., Horton, T. E., Grant, C. V., Hoogstraten, C. G., Britt, R. D., and DeRose, V. J. (1999) Mn2+-Nitrogen Interactions in RNA Probed by Electron Spin-Echo Envelope Modulation Spectroscopy: Application to the Hammerhead Ribozyme. *J. Am. Chem. Soc. 121*, 9215−9218.

(26) Horton, T. E., and DeRose, V. J. (2000) Cobalt Hexammine Inhibition of the Hammerhead Ribozyme. *Biochemistry 39*, 11408−11416.

(27) Seela, F., Debelak, H., Andrews, L., and Beigelman, L. (2003) Synthesis and enzymic hydrolysis of oligoribonucleotides incorporating 3-deazaguanosine: the importance of the nitrogen-3 atom of single conserved guanosine residues on the catalytic activity of the hammerhead ribozyme. *Helv. Chim. Acta 86*, 2726−2740.

(28) Suzumura, K., Takagi, Y., Orita, M., and Taira, K. (2004) NMR-Based Reappraisal of the Coordination of a Metal Ion at the Pro- Rp Oxygen of the A9/G10.1 Site in a Hammerhead Ribozyme. *J. Am. Chem. Soc. 126*, 15504−15511.

(29) Osborne, E. M., Schaak, J. E., and Derose, V. J. (2005) Characterization of a native hammerhead ribozyme derived from schistosomes. *RNA 11*, 187−196.

(30) Han, J., and Burke, J. M. (2005) Model for General Acid-Base Catalysis by the Hammerhead Ribozyme: pH-Activity Relationships of G8 and G12 Variants at the Putative Active Site. *Biochemistry 44*, 7864−7870.

DOI: 10.1021/acs.biochem.6b01192
Biochemistry XXXX, XXX, XXX−XXX

(31) Roychowdhury-Saha, M., and Burke, D. H. (2006) Extra-ordinary rates of transition metal ion-mediated ribozyme catalysis. *RNA 12*, 1846−1852.
(32) Roychowdhury-Saha, M., and Burke, D. H. (2007) Distinct reaction pathway promoted by non-divalent-metal cations in a tertiary stabilized hammerhead ribozyme. *RNA 13*, 841−848.
(33) Przybilski, R., and Hammann, C. (2007) The tolerance to exchanges of the WatsonCrick base pair in the hammerhead ribozyme core is determined by surrounding elements. *RNA 13*, 1625−1630.
(34) Boots, J. L., Canny, M. D., Azimi, E., and Pardi, A. (2008) Metal ion specificities for folding and cleavage activity in the Schistosoma hammerhead ribozyme. *RNA 14*, 2212−2222.
(35) Chi, Y.-I., Martick, M., Lares, M., Kim, R., Scott, W. G., and Kim, S.-H. (2008) Capturing hammerhead ribozyme structures in action by modulating general base catalysis. *PLoS Biol. 6*, e234.
(36) Thomas, J. M., and Perrin, D. M. (2008) Probing General Base Catalysis in the Hammerhead Ribozyme. *J. Am. Chem. Soc. 130*, 15467−15475.
(37) Thomas, J. M., and Perrin, D. M. (2009) Probing general acid catalysis in the hammerhead ribozyme. *J. Am. Chem. Soc. 131*, 1135−1143.
(38) Osborne, E. M., Ward, W. L., Ruehle, M. Z., and DeRose, V. J. (2009) The identity of the nucleophile substitution may influence metal interactions with the cleavage site of the minimal hammerhead ribozyme. *Biochemistry 48*, 10654−10664.
(39) Ward, W. L., and Derose, V. J. (2012) Ground-state coordination of a catalytic metal to the scissile phosphate of a tertiary-stabilized Hammerhead ribozyme. *RNA 18*, 16−23.
(40) Schultz, E. P., Vasquez, E. E., and Scott, W. G. (2014) Structural and catalytic effects of an invariant purine substitution in the hammerhead ribozyme: implications for the mechanism of acid-base catalysis. *Acta Crystallogr., Sect. D: Biol. Crystallogr. 70*, 2256−2263.
(41) Leclerc, F., and Karplus, M. (2006) Two-metal-ion mechanism for hammerhead-ribozyme catalysis. *J. Phys. Chem. B 110*, 3395−3409.
(42) Lee, T.-S., Silva-Lopez, C., Martick, M., Scott, W. G., and York, D. M. (2007) Insight into the role of Mg^{2+} in hammerhead ribozyme catalysis from x-ray crystallography and molecular dynamics simulation. *J. Chem. Theory Comput. 3*, 325−327.
(43) Martick, M., Lee, T.-S., York, D. M., and Scott, W. G. (2008) Solvent structure and hammerhead ribozyme catalysis. *Chem. Biol. 15*, 332−342.
(44) Lee, T.-S., Silva Lopez, C., Giambaşu, G. M., Martick, M., Scott, W. G., and York, D. M. (2008) Role of Mg^{2+} in hammerhead ribozyme catalysis from molecular simulation. *J. Am. Chem. Soc. 130*, 3053−3064.
(45) Lee, T.-S., and York, D. M. (2008) Origin of mutational effects at the C3 and G8 positions on hammerhead ribozyme catalysis from molecular dynamics simulations. *J. Am. Chem. Soc. 130*, 7168−7169.
(46) Lee, T.-S., Giambaşu, G. M., Sosa, C. P., Martick, M., Scott, W. G., and York, D. M. (2009) Threshold Occupancy and Specific Cation Binding Modes in the Hammerhead Ribozyme Active Site are Required for Active Conformation. *J. Mol. Biol. 388*, 195−206.
(47) Leclerc, F. (2010) Hammerhead Ribozymes: True Metal or Nucleobase Catalysis? Where Is the Catalytic Power from? *Molecules 15*, 5389−5407.
(48) Wong, K.-Y., Lee, T.-S., and York, D. M. (2011) Active participation of the Mg^{2+} ion in the reaction coordinate of RNA self-cleavage catalyzed by the hammerhead ribozyme. *J. Chem. Theory Comput. 7*, 1−3.
(49) Chval, Z., Chvalova, D., and Leclerc, F. (2011) Modeling the RNA 2′OH Activation: Possible Roles of Metal Ion and Nucleobase as Catalysts in Self-Cleaving Ribozymes. *J. Phys. Chem. B 115*, 10943−10956.
(50) Bevilacqua, P. C. (2003) Mechanistic considerations for general acid-base catalysis by RNA: Revisiting the mechanism of the hairpin ribozyme. *Biochemistry 42*, 2259−2265.
(51) Heldenbrand, H., Janowski, P. A., Giambaşu, G., Giese, T. J., Wedekind, J. E., and York, D. M. (2014) Evidence for the role of active site residues in the hairpin ribozyme from molecular simulations along the reaction path. *J. Am. Chem. Soc. 136*, 7789−7792.
(52) Klein, D. J., Been, M. D., and Ferré-D'Amaré, A. R. (2007) Essential role of an active-site guanine in *glmS* ribozyme catalysis. *J. Am. Chem. Soc. 129*, 14858−14859.
(53) Zhang, S., Ganguly, A., Goyal, P., Bingaman, J. L., Bevilacqua, P. C., and Hammes-Schiffer, S. (2015) Role of the active site guanine in the*glmS* ribozyme self-cleavage mechanism: Quantum mechanical/molecular mechanical free energy simulations. *J. Am. Chem. Soc. 137*, 784−798.
(54) Suslov, N. B., DasGupta, S., Huang, H., Fuller, J. R., Lilley, D. M. J., Rice, P. A., and Piccirilli, J. A. (2015) Crystal structure of the Varkud satellite ribozyme. *Nat. Chem. Biol. 11*, 840−846.
(55) Liu, Y., Wilson, T. J., McPhee, S. A., and Lilley, D. M. J. (2014) Crystal structure and mechanistic investigation of the twister ribozyme. *Nat. Chem. Biol. 10*, 739−744.
(56) Gaines, C. S., and York, D. M. (2016) Ribozyme Catalysis with a Twist: Active State of the Twister Ribozyme in Solution Predicted from Molecular Simulation. *J. Am. Chem. Soc. 138*, 3058−3065.
(57) Ren, A., Vusurovic, N., Gebetsberger, J., Gao, P., Juen, M., Kreutz, C., Micura, R., and Patel, D. (2016) Pistol ribozyme adopts a pseudoknot fold facilitating site-specific in-line cleavage. *Nat. Chem. Biol. 12*, 702−708.
(58) Wang, S., Karbstein, K., Peracchi, A., Beigelman, L., and Herschlag, D. (1999) Identification of the Hammerhead Ribozyme Metal Ion Binding Site Responsible for Rescue of the Deleterious Effect of a Cleavage Site Phosphorothioate. *Biochemistry 38*, 14363−14378.
(59) Lippert, B. (2005) Alterations of Nucleaobase pKa Values upon Metal Coordination: Origins and Consequences. *Prog. Inorg. Chem. 54*, 385−447.
(60) Sigel, R. K. O., and Pyle, A. M. (2007) Alternative Roles for Metal Ions in Enzyme Catalysis and the Implications for Ribozyme Chemistry. *Chem. Rev. 107*, 97−113.
(61) Lippert, B. (2008) Ligand-pK_a shifts through metals: potential relevance to ribozyme chemistry. *Chem. Biodiversity 5*, 1455−1474.
(62) Leonarski, F., D'Ascenzo, L., and Auffinger, P. (2017) Mg^{2+} ions: do they bind to nucleobase nitrogens? *Nucleic Acids Res. 45*, 987−1004.
(63) Leonarski, F., D'Ascenzo, L., and Auffinger, P. (2016) Binding of metals to purine N7 nitrogen atoms and implications for nucleic acids: A CSD survey. *Inorg. Chim. Acta 452*, 82−89.
(64) Panteva, M. T., Giambasu, G. M., and York, D. M. (2015) Force field for Mg^{2+}, Mn^{2+}, Zn^{2+}, and Cd^{2+} ions that have balanced interactions with nucleic acids. *J. Phys. Chem. B 119*, 15460−15470.
(65) Giese, T. J., and York, D. M. (2016) Ambient-Potential Composite Ewald Method for ab Initio Quantum Mechanical/Molecular Mechanical Molecular Dynamics Simulation. *J. Chem. Theory Comput. 12*, 2611−2632.
(66) Frisch, M. J., et al. (2009) *Gaussian 09*, revision A.02, Gaussian, Inc., Wallingford, CT.
(67) Zhao, Y., and Truhlar, D. G. (2008) The M06 suite of density functionals for main group thermochemistry, thermochemical kinetics, noncovalent interactions, excited states, and transition elements: two new functionals and systematic testing of four M06-class functionals and 12 other functionals. *Theor. Chem. Acc. 120*, 215−241.
(68) Cossi, M., Barone, V., Cammi, R., and Tomasi, J. (1996) Ab initio study of solvated molecules: a new implementation of the polarizable continuum model. *Chem. Phys. Lett. 255*, 327−335.
(69) Barone, V., Cossi, M., and Tomasi, J. (1997) A new definition of cavities for the computation of solvation free energies by the polarizable contiuum model. *J. Chem. Phys. 107*, 3210−3221.
(70) Cossi, M., Scalmani, G., Rega, N., and Barone, V. (2002) New developments in the polarizable continuum model for quantum mechanical and classical calculations on molecules in solution. *J. Chem. Phys. 117*, 43−54.
(71) Scalmani, G., and Frisch, M. J. (2010) Continuous surface charge polarizable continuum models of solvation. I. General formalism. *J. Chem. Phys. 132*, 114110−114124.

DOI: 10.1021/acs.biochem.6b01192
Biochemistry XXXX, XXX, XXX−XXX

(72) Rappé, A. K., Casewit, C. J., Colwell, K. S., Goddard, W. A., III, and Skiff, W. M. (1992) UFF, a full periodic table force field for molecular mechanics and molecular dynamics simulations. *J. Am. Chem. Soc. 114*, 10024−10035.
(73) Sigel, R. K. O., and Sigel, H. (2010) A stability concept for metal ion coordination to single-stranded nucleic acids and affinities of individual sites. *Acc. Chem. Res. 43*, 974−984.
(74) Weinhold, F., and Carpenter, J. E. (1988) in *The Structure of Small Molecules and Ions* (Naaman, R., and Vager, Z., Eds.) pp 227−236, Springer, Boston.
(75) Dolg, M., Wedig, U., Stoll, H., and Preuss, H. (1987) Energy-sdjusted ab initio pseudopotentials for the first row trasition elements. *J. Chem. Phys. 86*, 866−872.
(76) Sanli, S., Altun, Y., and Guven, G. (2014) Solvent Effects on pK_a Values of Some Anticancer Agents in Acetonitrile-Water Binary Mixtures. *J. Chem. Eng. Data 59*, 4015−4020.
(77) Case, D. A., et al. (2014) *AMBER 14*, University of California, San Francisco, San Francisco.
(78) Horn, H. W., Swope, W. C., Pitera, J. W., Madura, J. D., Dick, T. J., Hura, G. L., and Head-Gordon, T. (2004) Development of an improved four-site water model for biomolecular simulations: TIP4P-Ew. *J. Chem. Phys. 120*, 9665−9678.
(79) Cornell, W. D., Cieplak, P., Bayly, C. I., Gould, I. R., Merz, K. M., Jr., Ferguson, D. M., Spellmeyer, D. C., Fox, T., Caldwell, J. W., and Kollman, P. A. (1995) A second generation force field for the simulation of proteins, nucleic acids and organic molecules. *J. Am. Chem. Soc. 117*, 5179−5197.
(80) Maier, J. A., Martinez, C., Kasavajhala, K., Wickstrom, L., Hauser, K. E., and Simmerling, C. (2015) ff14SB: Improving the Accuracy of Protein Side Chain and Backbone Parameters from ff99SB. *J. Chem. Theory Comput. 11*, 3696−3713.
(81) Pérez, A., Marchán, I., Svozil, D., Sponer, J., Cheatham, T. E., III, Laughton, C. A., and Orozco, M. (2007) Refinement of the AMBER force field for nucleic acids: Improving the description of α/γconformers. *Biophys. J. 92*, 3817−3829.
(82) Zgarbová, M., Otyepka, M., Šponer, J., Mládek, A., Banáš, P., Cheatham, T. E., III, and Jurečka, P. (2011) Refinement of the Cornell et al. nucleic acids force field based on reference quantum chemical calculations of glycosidic torsion profiles. *J. Chem. Theory Comput. 7*, 2886−2902.
(83) Joung, I. S., and Cheatham, T. E., III (2008) Determination of alkali and halide monovalent ion parameters for use in explicitly solvated biomolecular simulations. *J. Phys. Chem. B 112*, 9020−9041.
(84) Li, P., and Merz, K. M., Jr. (2014) Taking into account the ion-induced dipole interaction in the nonbonded model of ions. *J. Chem. Theory Comput. 10*, 289−297.
(85) Panteva, M. T., Giambaşu, G. M., and York, D. M. (2015) Comparison of structural, thermodynamic, kinetic and mass transport properties of Mg^{2+} ion models commonly used in biomolecular simulations. *J. Comput. Chem. 36*, 970−982.
(86) Essmann, U., Perera, L., Berkowitz, M. L., Darden, T., Lee, H., and Pedersen, L. G. (1995) A smooth particle mesh Ewald method. *J. Chem. Phys. 103*, 8577−8593.
(87) Steinbrecher, T., Joung, I., and Case, D. A. (2011) Soft-Core Potentials in Thermodynamic Integration: Comparing One- and Two-Step Transformations. *J. Comput. Chem. 32*, 3253−3263.
(88) Bayly, C. I., Cieplak, P., Cornell, W. D., and Kollman, P. A. (1993) A Well-Behaved Electrostatic Potential Based Method Using Charge Restraints for Deriving Atomic Charges: The RESP Model. *J. Phys. Chem. 97*, 10269−10280.
(89) Steinbrecher, T., Mobley, D. L., and Case, D. A. (2007) Nonlinear scaling schemes for Lennard-Jones interactions in free energy calculations. *J. Chem. Phys. 127*, 214108.
(90) Perdew, J. P., Burke, K., and Ernzerhof, M. (1996) Generalized gradient approximation made simple. *Phys. Rev. Lett. 77*, 3865−3868.
(91) Adamo, C., and Barone, V. (1999) Toward reliable density functional methods without adjustable parameters: the PBE0 model. *J. Chem. Phys. 110*, 6158−6170.
(92) Lee, T.-S., Radak, B. K., Pabis, A., and York, D. M. (2013) A new maximum likelihood approach for free energy profile construction from molecular simulations. *J. Chem. Theory Comput. 9*, 153−164.
(93) Wilson, T. J., and Lilley, D. M. (2013) A Mechanistic Comparison of the Varkud Satellite and Hairpin Ribozymes. *Prog. Mol. Biol. Transl. Sci. 120*, 93−121.
(94) Krishnamurthy, R. (2012) Role of pKa of Nucleobases in the Origins of Chemical Evolution. *Acc. Chem. Res. 45*, 2035−2044.
(95) Corona-Martinez, D. O., Gomez-Tagle, P., and Yatsimirsky, A. K. (2012) Electrophilic Assistance to the Cleavage of an RNA Model Phopshodiester via Specific and General Base-Catalyzed Mechanisms. *J. Org. Chem. 77*, 9110−9119.
(96) Xin, Y., and Hamelberg, D. (2010) Deciphering the role of glucosamine-6-phosphate in the riboswitch action of glmS ribozyme. *RNA 16*, 2455−2463.
(97) Murray, J. B., Seyhan, A. A., Walter, N. G., Burke, J. M., and Scott, W. G. (1998) The hammerhead, hairpin and VS ribozymes are catalytically proficient in monovalent cations alone. *Chem. Biol. 5*, 587−595.
(98) Curtis, E. A., and Bartel, D. P. (2001) TThe hammerhead cleavage reaction in monovalent cations. *RNA 7*, 546−552.
(99) O'Rear, J. L., Wang, S., Feig, A. L., Beigelman, L., Uhlenbeck, O. C., and Herschlag, D. (2001) Comparison of the hammerhead cleavage reactions stimulated by monovalent and divalent cations. *RNA 7*, 537−545.
(100) Frankel, E. A., Strulson, C. A., Keating, C. D., and Bevilacqua, P. C. (2017) Cooperative interactions in the hammerhead ribozyme drive pK_a shifting of G12 and its stacked base C17. *Biochemistry 56*, 2537−2548.
(101) Swift, R. V., Ong, C. D., and Amaro, R. E. (2012) Magnesium-Induced Nucleophile Activation in the Guanylyltransferase mRNA Capping Enzyme. *Biochemistry 51*, 10236−10243.
(102) Radak, B. K., Lee, T.-S., Harris, M. E., and York, D. M. (2015) Assessment of metal-assisted nucleophile activation in the hepatitis delta virus ribozyme from molecular simulation and 3D-RISM. *RNA 21*, 1566−1577.
(103) Lopata, A., Jambrina, P. G., Sharma, P. K., Brooks, B. R., Tóth, J., Vértessy, B. G., and Rosta, E. (2015) Mutations Decouple Proton Transfer from Phosphate Cleavage in the dUTPase Catalytic Reaction. *ACS Catal. 5*, 3225−3237.
(104) Nagy, G. N., Suardíaz, R., Lopata, A., Ozohanics, O., Vékey, K., Brooks, B. R., Leveles, I., Tóth, J., Vértessy, B. G., and Rosta, E. (2016) Structural Characterization of Arginine Fingers: Identification of an Arginine Finger for the Pyrophosphatase dUTPases. *J. Am. Chem. Soc. 138*, 15035−15045.

DOI: 10.1021/acs.biochem.6b01192
Biochemistry XXXX, XXX, XXX−XXX